Electrical control of the RKKY interaction in bilayer graphene

N. Klier,[1] S. Sharma,[2] O. Pankratov,[1] and S. Shallcross[1,*]
[1]*Lehrstuhl für Theoretische Festkörperphysik, Staudtstrasse 7-B2, 91058 Erlangen, Germany*
[2]*Max-Planck-Institut fur Mikrostrukturphysik Weinberg 2, D-06120 Halle, Germany*
(Received 11 July 2016; revised manuscript received 28 October 2016; published 28 November 2016)

The Ruderman-Kittel-Kasuya-Yosida (RKKY) interaction between impurity spins is calculated for bilayer graphene in the presence of a layer symmetry-breaking external electric field. We find that for intercalated impurities (i.e., impurity atoms between the two constituent layers of the bilayer) the interaction is extraordinarily sensitive to such a field. In particular, (i) the form of the RKKY interaction may be tuned between oscillatory, ferromagnetic, and antiferromagnetic simply by varying the external field, and (ii) the strength of the RKKY interaction may be increased by an order of magnitude by application of an external field. This sensitivity arises directly from the "Mexican hat" form that the low-energy spectrum takes in an applied field. These finding suggest that heterostructures of intercalated magnetic atoms in bilayer graphene may represent a possible system for electrical control over magnetic structure.

DOI: 10.1103/PhysRevB.94.205436

I. INTRODUCTION

The Ruderman-Kittel-Kasuya-Yosida (RKKY) interaction [1–3] in graphene [4–26] possesses a number of features that render it very different from the familiar RKKY interaction found, for example, on the (111) surface of Cu [27]. These differences arise from two distinct features of the electronic structure: the multivalley nature of the low-energy spectrum and the Dirac-Weyl cones situated at each of these valleys. The former leads to anisotropic fast oscillations in the RKKY interaction [4,10,14,25], while the latter is responsible for an unusual R^{-3} asymptotic decay of the interaction when the Fermi energy coincides with the Dirac point [4,10,14].

The AB-stacked graphene bilayer, a prototypical example of a van der Waals heterostructure, also features a novel RKKY interaction [5,15,16,21,25]. In particular, it was recently shown that intercalated impurities—that occupy the open spaces between the layers of the bilayer (see Fig. 1)–have a remarkably rich behavior close to the band edges of the high-energy bonding and antibonding bands, where a sudden transition of the RKKY interaction from oscillatory to antiferromagnetic occurs [25].

This interesting RKKY physics of graphene and bilayer graphene arises directly from the form of the single-particle band structure in these materials, suggesting that modification of the electronic structure by external variables, such as an electric field or strain, may have interesting consequences for the RKKY interaction. One of the most well-known such effects is the opening of a band gap in bilayer graphene by application of a layer symmetry-breaking electric field [28–31], which has been shown to sensitively impact the RKKY interaction in bilayer graphene leading to a ferromagnetic to antiferromagmetic switching for plaquette impurities [15]. In this work we will explore the impact of such a field on the RKKY interaction of intercalated impurities, finding that it is highly sensitive to an applied electric field.

By tuning an electric field such that the band edge moves from below to above the Fermi energy we show that the RKKY interaction evolves from oscillatory at low bias, to antiferromagnetic, and finally when the Fermi energy is in the gap, to ferromagnetic. Close to the gap edge the low-energy band manifold resembles that of a "Mexican hat," and this energy region is associated with an order of magnitude increase in the strength of the RKKY interaction. Finally, if the Fermi energy is pinned in the band gap, yet is not too far from the gap edge, finite-temperature calculations reveal a most unusual change in the RKKY interaction as a function of temperature. We find that the interaction changes its qualitative form with temperature but does not significantly reduce in strength: A low-temperature ($T < 50$ K) ferromagnetic interaction goes over to a antiferromagnetic interaction at room temperature.

II. THEORY

A. Basic theory and notation

Formalism of the RKKY interaction. The coupling of two impurity spins to the itinerant Dirac gas is described by the Hamiltonian

$$H = H^0 - \lambda(\mathbf{S}_1 \cdot \mathbf{s}_1 + \mathbf{S}_2 \cdot \mathbf{s}_2), \tag{1}$$

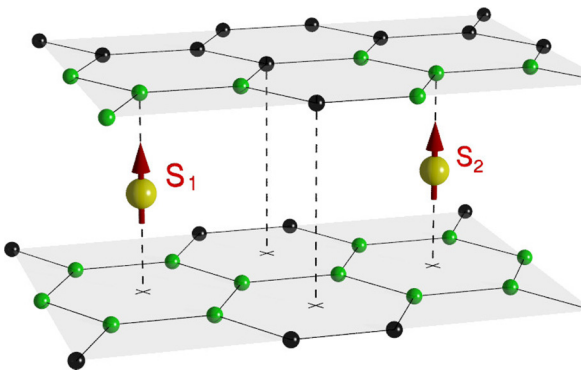

FIG. 1. Two intercalated impurities in AB-stacked bilayer graphene. Each impurity spin couples via a contact interaction to the ten surrounding carbon atoms of the bilayer (light shaded/green atoms).

*sam.shallcross@fau.de

where H^0 is the Hamiltonian of the biased bilayer system, $\mathbf{S}_i$ denotes the spin of the impurity, and $\mathbf{s}_i = \frac{\hbar}{2}\sum_{\mu,\nu} c^\dagger_{i\mu}\boldsymbol{\tau}_{\mu\nu}c_{i\nu}$ is taken for the itinerant quasiparticle spin density. By convention, the operator $c^\dagger_{i\mu}$ generates an quasiparticle at site i with spin μ and $\boldsymbol{\tau}$ represents the vector of Pauli matrices. The interaction energy between two impurities that are separated by the distance vector $\mathbf{R} = (R,\theta) = \mathbf{r}' - \mathbf{r}$ is given by the well-known expression

$$E^{RKKY} = (\mathbf{S}_1 \cdot \mathbf{S}_2) J_{\alpha_l\alpha'_{l'}}(\mathbf{R}). \tag{2}$$

Note that the index $\alpha \in \{A,B\}$ stands for the sublattice and $l \in \{1,2\}$ for the layer of each impurity. In the zero-temperature formalism the exchange integral $J_{\alpha_l\alpha'_{l'}}(\mathbf{R})$ is given by the expression

$$J_{\alpha_l\alpha'_{l'}}(\mathbf{R}) = -\frac{\lambda^2\hbar^2}{2\pi}\int_{-\infty}^{E_F} dE\,\mathrm{Im}\big[G^0_{\alpha_l\alpha'_{l'}}(-\mathbf{R},E) \times G^0_{\alpha'_{l'}\alpha_l}(\mathbf{R},E)\big], \tag{3}$$

where $G^0_{\alpha'_{l'}\alpha_l}(\mathbf{R},E)$ is the Dirac gas propagator at zero temperature. Additionally, we will discuss the effects of finite temperature on the RKKY interaction for which the appropriate expression is the Matsubara sum

$$\mathcal{J}_{\alpha_l\alpha'_{l'}}(\mathbf{R}) = \frac{\lambda^2}{2\beta}\sum_n \mathcal{G}^0_{\alpha_l\alpha'_{l'}}(-\mathbf{R},i\omega_n)\mathcal{G}^0_{\alpha'_{l'}\alpha_l}(\mathbf{R},i\omega_n), \tag{4}$$

where $\mathcal{G}^0_{\alpha_l\alpha'_{l'}}(\mathbf{R},i\omega_n)$ is the finite-temperature propagator in real space, and where we have introduced the Matsubara frequency $\omega_n = (2n+1)\pi/(\hbar\beta)$, with $\beta = 1/(k_BT)$ and the Boltzmann constant k_B.

Hamiltonian. Bilayer graphene consists of two graphene layers in an AB-stacked (graphitic) configuration. In this work we consider the simplest possible tight-binding scheme of (i) a nearest-neighbor hopping in plane and (ii) interlayer hopping only along the bonding vector. The strength of this interlayer coupling is described by the constant $t_\perp$, which has a value of $\approx$0.38 eV. Additionally, we apply a layer symmetry-breaking bias voltage V between both layers. Note that as a consequence of our simple choice of tight-binding scheme we do not capture the three satellite Dirac points which trigonally decorate the K-centered Dirac point, for which momentum-dependent layer off-diagonal blocks in the Hamiltonian are required. Including these low-energy Dirac points may change details of the RKKY interaction in the Mexican hat region, but will certainly not change the qualitative features of the field dependence of the RKKY that we will describe here, and for that reason we omit this detail of the spectrum.

In a low-energy expansion close to the mth corner of the hexagonal Brillouin zone we find the Hamiltonian of the biased bilayer is given by

$$H^0_m(\mathbf{k}) = \begin{pmatrix} \frac{V}{2} & \tilde{\Phi}_m(\mathbf{k}) & -t_\perp & 0 \\ \tilde{\Phi}^*_m(\mathbf{k}) & \frac{V}{2} & 0 & 0 \\ -t_\perp & 0 & -\frac{V}{2} & \tilde{\Phi}^*_m(\mathbf{k}) \\ 0 & 0 & \tilde{\Phi}_m(\mathbf{k}) & -\frac{V}{2} \end{pmatrix}, \tag{5}$$

where $\tilde{\Phi}_m(\mathbf{k}) = \hbar v_F k e^{i(\gamma_m+\delta_m\phi_\mathbf{k})}$, with $\phi_\mathbf{k} = \tan^{-1} k_y/k_x$, and v_F is the Fermi velocity of the Dirac cone. The two phases δ_m and γ_m depend on the particular high-symmetry K-point used for the expansion and are given in Table I; for the relation between the high-symmetry $\mathbf{K}_m$ point and the graphene Brillouin zone, see Fig. 2. Diagonalization of the Hamiltonian Eq. (5) leads to the four energy bands described by the eigenvalues

$$E_{\sigma_1\sigma_2}(\mathbf{k}) = \sigma_1\left[v_F^2k^2 + \frac{t_\perp^2}{2} + \frac{V^2}{4} + \sigma_2\sqrt{\frac{t_\perp^2}{4} + v_F^2k^2(t_\perp^2+V^2)}\right]^{1/2}, \tag{6}$$

where $\sigma_1 = \pm1$ and $\sigma_2 = \pm1$ label the four bands of bilayer graphene.

TABLE I. Coefficients for the low-energy expansion at each of the six high-symmetry K points of the graphene Brillouin zone.

	$\mathbf{K}_1$	$\mathbf{K}_2$	$\mathbf{K}_3$	$\mathbf{K}_4$	$\mathbf{K}_5$	$\mathbf{K}_6$
γ_m	0	π	$-\frac{\pi}{3}$	$\frac{2\pi}{3}$	$\frac{\pi}{3}$	$-\frac{2\pi}{3}$
δ_m	-1	$+1$	$+1$	-1	$+1$	-1

B. RKKY interaction at $T = 0$

1. Green's function

The full real-space Green's function is given by

$$G^0(\mathbf{R},E) = \frac{1}{3}\sum_{m=1}^{6} G^0_m(\mathbf{R},E)e^{i\mathbf{K}_m\cdot\mathbf{R}}, \tag{7}$$

where we have introduced $G^0_m(\mathbf{R},E)$ that may be obtained from a Fourier transform of the retarded momentum space Green's function $G^0_m(\mathbf{k},E) = [E + i\eta - H^0_m(\mathbf{k})]^{-1}$. The real-space Green's function at the mth K point is given by the expression

$$G^0_m(\mathbf{R},E) = -\frac{i\pi^2}{8\hbar^2v_F^2\Omega_{BZ}u}M(\mathbf{R},E), \tag{8}$$

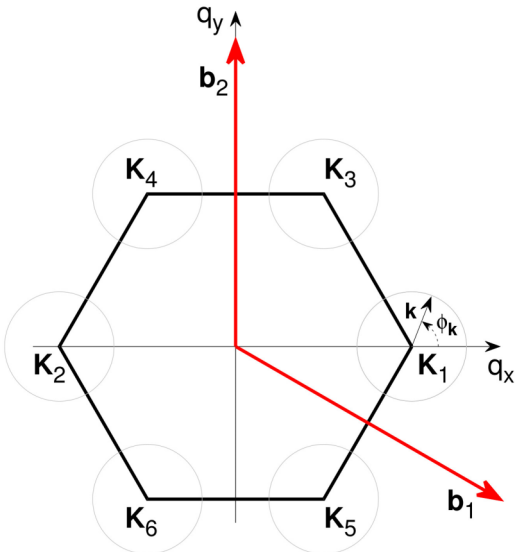

FIG. 2. Hexagonal Brillouin zone of bilayer graphene with the high-symmetry K-points labeled.

TABLE II. Elements of the $T = 0$ Green's function of bilayer graphene in the presence of a layer symmetry-breaking field. The function $\Phi_m(\mathbf{R}) = e^{i(\gamma_m+\delta_m\theta)}$ with the parameters γ_m and δ_m are given Table II.

$\alpha_l\alpha'_{l'}$	$M_{\alpha_l\alpha'_{l'}}(\mathbf{R},E)$
A_1A_1	$2B(-V)[A(-V)H_0^1(z^+R) + A(V)H_0^1(z^-R)]$
A_1B_1	$4i\hbar v_F\Phi_m(\mathbf{R})[A(-V)z^+H_1^1(z^+R) + A(V)z^-H_1^1(z^-R)]$
A_1A_2	$t_\perp B(V)B(-V)[H_0^1(z^+R) - H_0^1(z^-R)]$
A_1B_2	$2i\hbar v_F\Phi_m^*(\mathbf{R})t_\perp B(-V)[z^+H_1^1(z^+R) - z^-H_1^1(z^-R)]$
B_1B_1	$2B(-V)[F_+(V)H_0^1(z^+R) + F_-(V)H_0^1(z^-R)]$
B_1A_2	$2i\hbar v_F\Phi_m^*(\mathbf{R})t_\perp B(V)[z^+H_1^1(z^+R) - z^-H_1^1(z^-R)]$
B_1B_2	$-4\hbar^2v_F^2\Phi_m^{*2}(\mathbf{R})t_\perp[z^{+2}H_2^1(z^+R) - z^{-2}H_2^1(z^-R)]$
A_2A_2	$2B(V)[A(V)H_0^1(z^+R) + A(-V)H_0^1(z^-R)]$
A_2B_2	$4i\hbar v_F\Phi_m^*(\mathbf{R})[A(V)z^+H_1^1(z^+R) + A(-V)z^-H_1^1(z^-R)]$
B_2B_2	$2B(V)[F_+(-V)H_0^1(z^+R) + F_-(-V)H_0^1(z^-R)]$

where Ω_{BZ} stands for the area of the Brillouin zone and the elements of the matrix $M(\mathbf{R},E)$ are presented in Table II. We have introduced in the expressions of this table the functions of the interlayer bias,

$$A(V) = u + (E+i\eta)V, \tag{9}$$

$$B(V) = 2(E+i\eta) + V, \tag{10}$$

$$F_s(V) = u - s(E+i\eta)V + s\frac{2(E+i\eta)+V}{2(E+i\eta)-V}t_\perp^2, \tag{11}$$

with $s \in \{\pm\}$ and u defined as follows:

$$u = \sqrt{(E+i\eta)^2(V^2+t_\perp^2) - V^2t_\perp^2/4}. \tag{12}$$

The arguments of the Hankel functions, z^+R and z^-R, are given by

$$z^+ = \frac{1}{\hbar v_F}\sqrt{(E+i\eta)^2 + \frac{V^2}{4} + u}, \tag{13}$$

$$z^- = \frac{1}{\hbar v_F}\sqrt{(E+i\eta)^2 + \frac{V^2}{4} - u}. \tag{14}$$

By definition, the square roots in Eqs. (12), (13), and (14) are taken so that the imaginary part is positive valued. Taking the $\eta \to 0$ limit of u, z^+, and z^- yields

$$z^+|_{\eta\to0} = \frac{1}{\hbar v_F}\mathrm{sgn}\left(E + \frac{\sqrt{V^2+4t_\perp^2}}{2}\right)\sqrt{E^2 + \frac{V^2}{4} + u}, \tag{15}$$

$$z^-|_{\eta\to0} = \frac{1}{\hbar v_F}\mathrm{sgn}\left(E - \frac{V}{2}\right)\sqrt{E^2 + \frac{V^2}{4} - u}, \tag{16}$$

$$u|_{\eta\to0} = \mathrm{sgn}\left(E + \frac{Vt_\perp}{2\sqrt{V^2+t_\perp^2}}\right) \times \sqrt{E^2(V^2+t_\perp^2) - \frac{V^2t_\perp^2}{4}}. \tag{17}$$

In the limit $V \to 0$ and $\eta \to 0$ these functions take the following simple forms: $A(0) = Et_\perp$, $B(0) = 2E$, $F_s(0) = t_\perp(E + st_\perp)$, $u = Et_\perp$, $z^+ = \mathrm{sgn}(E+t_\perp)\sqrt{E^2+Et_\perp}/(\hbar v_F)$, and $z^- = \mathrm{sgn}(E)\sqrt{E^2-Et_\perp}/(\hbar v_F)$. Hence, we recover under these circumstances the Green's function that was found for the bilayer without bias [25].

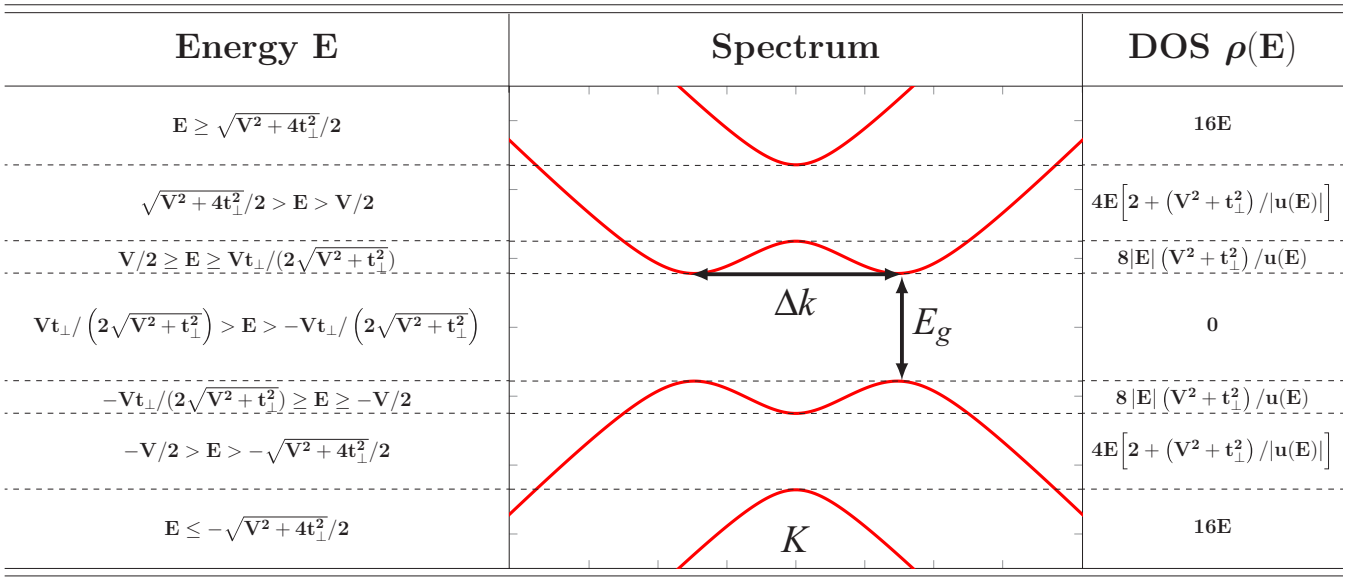

FIG. 3. The total density of states of biased bilayer graphene $\rho(E) = \sum_i \rho_i(E)$ (right) and a schematic illustration of the low-energy spectrum in vicinity of the K point (middle). The two low-energy bands are separated by a band gap $E_g = Vt_\perp/\sqrt{V^2+t_\perp^2}$ and the distance between the two minima (maxima) is given by $\Delta k = V\sqrt{(V^2+2t_\perp^2)/(V^2+t_\perp^2)}/(2\hbar v_F)$. The DOS is defined piecewise in the energy intervals on the left. The function $u(E)$ must be inserted in its $\eta \to 0$ limit as defined in Eq. (17).

TABLE III. The density of states of biased bilayer graphene on sites A_1, B_1, A_2, and B_2. The energy range of applicability of each expression is indicated by the expression at the top of each column. The function $u(E)$ must be inserted in the $\eta \to 0$ limit as defined in Eq. (17).

	$\lvert E\rvert < \frac{Vt_\perp}{2\sqrt{V^2+t_\perp^2}}$	$\frac{Vt_\perp}{2\sqrt{V^2+t_\perp^2}} \leqslant \lvert E\rvert \leqslant \frac{V}{2}$	$\frac{V}{2} < \lvert E\rvert < \sqrt{\frac{V^2}{4}+t_\perp^2}$	$\lvert E\rvert \geqslant \sqrt{\frac{V^2}{4}+t_\perp^2}$
$\rho_{A_1}(E)$	0	$-2\frac{\lvert E\rvert V}{u(E)}(2E-V)$	$(2E-V)[1-\frac{\lvert E\rvert V}{u(E)}]$	$2(2E-V)$
$\rho_{B_1}(E)$	0	$-2\frac{\mathrm{sgn}(E)}{u(E)}[(2E-V)EV-(2E+V)t_\perp^2]$	$(2E-V)[1-\frac{EV}{\lvert u(E)\rvert}]+\frac{t_\perp^2}{\lvert u(E)\rvert}(2E+V)$	$2(2E-V)$
$\rho_{A_2}(E)$	0	$2\frac{\lvert E\rvert V}{u(E)}(2E+V)$	$(2E+V)[1+\frac{\lvert E\rvert V}{u(E)}]$	$2(2E+V)$
$\rho_{B_2}(E)$	0	$2\frac{\mathrm{sgn}(E)}{u(E)}[(2E+V)EV+(2E-V)t_\perp^2]$	$(2E+V)[1+\frac{EV}{\lvert u(E)\rvert}]+\frac{t_\perp^2}{\lvert u(E)\rvert}(2E-V)$	$2(2E+V)$

2. *Density of states*

The density of states (DOS) on site $\alpha \in \{A,B\}$ and layer $l \in \{1,2\}$ may be obtained from the real-space Green's function by

$$D_{\alpha_l}(E) = -\frac{1}{\pi}\lim_{R\to 0}\mathrm{Im}\big[G^0_{\alpha_l\alpha_l}(\mathbf{R},E)\big]. \tag{18}$$

Surprisingly, given the rather complex form of the Green's function, this expression can be manipulated to yield a very compact analytical form for the DOS of the bilayer in the presence of a layer symmetry-breaking electric field. This expression is useful for model work and appears not to have been noticed before (a more complex expression involving elliptical functions can be found in the appendix of Ref. [31]). In the low-energy band structure in the vicinity of the K point, shown in Fig. 3, there are four regions to distinguish: the band gap around the K point, the Mexican hat region, the gap between the low- and the high-energy bands, and, finally, at high energies, the two-band region. In these four regions the argument of the Green's function z^+ or z^- is either purely real, purely imaginary, or complex and this has dramatic consequences on the form of the DOS. Use of the Sokhotski-Plemelj theorem and the identity $\lim_{R\to 0}\mathrm{Im}[iH_0^1(z^\pm R)] = \mathrm{sgn}(z^\pm)$ allows one to obtain an expression for the density of states at site α of layer l

$$D_{\alpha_l}(E) = \mathrm{sgn}(E)\frac{\pi}{4\hbar^2 v_F^2\Omega_{BZ}}\rho_{\alpha_l}(E), \tag{19}$$

where $\rho_{\alpha_l}(E)$ is given by Table III. The total density of states, $D(E) = \sum_{\alpha,l} D_{\alpha_l}(E)$, is shown in the last column in Fig. 3.

3. *Number of states*

The number of occupied states and the density of states are connected by integration: $N(E_F) = \int_{-\infty}^{E_F} dE\, D(E)$. After making use of particle-hole symmetry, $D(E) = D(-E)$, the number of states can be rewritten as

$$N(E_F) = N_0 + \mathrm{sgn}(E_F)\Delta N(E_F), \tag{20}$$

where we defined the constant N_0, equal to number of states at Dirac point, and the function $\Delta N(E_F) = \int_0^{|E_F|} dE\, D(E)$. With help of $D(E)$, given by the last column of Fig. 3, we may calculate the integral $\Delta N(E_F)$, finding

$$\Delta N(E_F) = \frac{\pi}{\hbar^2 v_F^2\Omega_{BZ}}\xi(E_F), \tag{21}$$

with the function $\xi(E_F)$ defined by Table IV. This expression may easily be inverted to obtain the Fermi energy given a fixed particle density and bias. In the calculation of the RKKY interaction at fixed particle density this analytical procedure significantly improves the efficiency of the calculation.

4. *RKKY interaction*

In order to calculate the exchange integral, we use Eq. (3) and insert the Green's function given by Eq. (8). As shown in previous works [4,10,14,25] the exchange integral separates into the product of an intravalley and intervalley terms and so can be written as

$$J_{\alpha_l\alpha'_{l'}}(\mathbf{R}) = CI_{\alpha_l\alpha'_{l'}}(R)f_{\alpha_l\alpha'_{l'}}(\mathbf{R}), \tag{22}$$

with $C = -\frac{\lambda^2\hbar^2a^2}{64\pi t^2}$. In the absence of bias there are six inequivalent substitutional RKKY interactions [25]; however, due to the symmetry breaking by the applied bias this becomes 10 distinct functions $J_{\alpha_l\alpha'_{l'}}(\mathbf{R})$ (the maximum possible), which we present in Table V. From the expressions in Table V it is now clear that the functions defined in Eqs. (9) to (12) encode the layer symmetry breaking of the bias potential as they always occur in $\pm$ combinations, which in the limit $V \to 0$ for each case become a simple multiplicative factor for the I function. The intervalley part of the interaction is much the simpler part of the RKKY and is always defined by the three functions,

$$f_{A_1A_1}(\mathbf{R}) = 1+\cos[2\mathbf{K}_2\cdot\mathbf{R}], \tag{23}$$

$$f_{B_1A_1}(\mathbf{R}) = 1+\cos[2\mathbf{K}_2\cdot\mathbf{R}+\pi-2\theta], \tag{24}$$

$$f_{B_2B_1}(\mathbf{R}) = 1+\cos[2\mathbf{K}_2\cdot\mathbf{R}+4\theta], \tag{25}$$

where θ is the polar angle of the vector $\mathbf{R}$. The relevant member of these three functions for each type of substitutional RKKY interaction is also shown in Table V. Note that this intervalley

TABLE IV. Number of states function $\xi(E_F)$. The function $u(E_F)$ must be inserted in its $\eta \to 0$ limit.

Fermi energy range	$\xi(E_F)$
$\lvert E_F\rvert \geqslant \sqrt{\frac{V^2}{4}+t_\perp^2}$	$2(E_F^2+\frac{V^2}{4})$
$\sqrt{\frac{V^2}{4}+t_\perp^2} > \lvert E_F\rvert > \frac{V}{2}$	$E_F^2+\frac{V^2}{4}+\lvert u(E_F)\rvert$
$\frac{V}{2} \geqslant \lvert E_F\rvert \geqslant \frac{Vt_\perp}{2\sqrt{V^2+t_\perp^2}}$	$2\lvert u(E_F)\rvert$
$\lvert E_F\rvert < \frac{Vt_\perp}{2\sqrt{V^2+t_\perp^2}}$	0

TABLE V. Intralayer part of the RKKY interaction at $T = 0$; the expression for the full RKKY interaction is given in Eq. (22).

$\alpha_l\alpha'_{l'}$	$I_{\alpha_l\alpha'_{l'}}(R)$	$f_{\alpha\alpha'}(\mathbf{R})$
A_1A_1	$\frac{1}{4\hbar^2v_F^2}\int_{E_F}^{\infty} dE\,\mathrm{Im}\{\frac{B(-V)^2}{u^2}[A(-V)H_0^1(z^+R)+A(V)H_0^1(z^-R)]^2\}$	$f_{A_1A_1}(\mathbf{R})$
A_2A_2	$\frac{1}{4\hbar^2v_F^2}\int_{E_F}^{\infty} dE\,\mathrm{Im}\{\frac{B(V)^2}{u^2}[A(V)H_0^1(z^+R)+A(-V)H_0^1(z^-R)]^2\}$	$f_{A_1A_1}(\mathbf{R})$
B_1B_1	$\frac{1}{4\hbar^2v_F^2}\int_{E_F}^{\infty} dE\,\mathrm{Im}\{\frac{B(-V)^2}{u^2}[F_+(V)H_0^1(z^+R)+F_-(V)H_0^1(z^-R)]^2\}$	$f_{A_1A_1}(\mathbf{R})$
B_2B_2	$\frac{1}{4\hbar^2v_F^2}\int_{E_F}^{\infty} dE\,\mathrm{Im}\{\frac{B(V)^2}{u^2}[F_+(-V)H_0^1(z^+R)+F_-(-V)H_0^1(z^-R)]^2\}$	$f_{A_1A_1}(\mathbf{R})$
B_1A_1	$\int_{E_F}^{\infty} dE\,\mathrm{Im}\{\frac{1}{u^2}[A(-V)z^+H_1^1(z^+R)+A(V)z^-H_1^1(z^-R)]^2\}$	$f_{B_1A_1}(\mathbf{R})$
A_2B_2	$\int_{E_F}^{\infty} dE\,\mathrm{Im}\{\frac{1}{u^2}[A(V)z^+H_1^1(z^+R)+A(-V)z^-H_1^1(z^-R)]^2\}$	$f_{B_1A_1}(\mathbf{R})$
B_2A_1	$\frac{t_\perp^2}{4}\int_{E_F}^{\infty} dE\,\mathrm{Im}\{\frac{B(-V)^2}{u^2}[z^+H_1^1(z^+R)-z^-H_1^1(z^-R)]^2\}$	$f_{B_1A_1}(-\mathbf{R})$
A_2B_1	$\frac{t_\perp^2}{4}\int_{E_F}^{\infty} dE\,\mathrm{Im}\{\frac{B(V)^2}{u^2}[z^+H_1^1(z^+R)-z^-H_1^1(z^-R)]^2\}$	$f_{B_1A_1}(-\mathbf{R})$
A_2A_1	$\frac{t_\perp^2}{16\hbar^2v_F^2}\int_{E_F}^{\infty} dE\,\mathrm{Im}\{\frac{B(V)B(-V)}{u^2}[H_0^1(z^+R)-H_0^1(z^-R)]^2\}$	$f_{A_1A_1}(\mathbf{R})$
B_2B_1	$\hbar^2v_F^2t_\perp^2\int_{E_F}^{\infty} dE\,\mathrm{Im}\{\frac{1}{u^2}[z^{+2}H_2^1(z^+R)-z^{-2}H_2^1(z^-R)]^2\}$	$f_{B_2B_1}(\mathbf{R})$

scattering cannot change the sign of the RKKY interaction and that the periodicity of these functions, and the fact that $\mathbf{R}$ must be a lattice vector $\mathbf{R} = n_1\mathbf{a}_1 + n_2\mathbf{a}_2$ with $n_i \in \mathbb{Z}$, ensure trigonal symmetry of Eqs. (23)–(25).

C. RKKY interaction at finite temperature

1. Green's function

The finite-temperature Green's function in momentum space is defined by $\mathcal{G}^0(\mathbf{k},i\omega_n) = [i\hbar\omega_n + \mu - H^0(\mathbf{k})]^{-1}$. After a Fourier transform we find the real-space Green's function,

$$\mathcal{G}^0(\mathbf{R},i\omega_n) = \frac{1}{3}\sum_{m=1}^{6}\mathcal{G}_m^0(\mathbf{R},i\omega_n)e^{i\mathbf{K}_m\cdot\mathbf{R}}, \tag{26}$$

where

$$\mathcal{G}_m^0(\mathbf{R},i\omega_n) = -\frac{i\pi^2}{8\hbar v_F^2\Omega_{BZ}u}\mathcal{M}(\mathbf{R},i\omega_n). \tag{27}$$

In this expression we have introduced the matrix $\mathcal{M}(\mathbf{R},i\omega_n)$, the elements of which are presented in Table VI and in which we have defined three functions of the interlayer bias, analogous to those of the $T = 0$ formalism,

$$\mathcal{A}(V) = u + [i\hbar\omega_n + \mu]V, \tag{28}$$

$$\mathcal{B}(V) = 2i\hbar\omega_n + 2\mu + V, \tag{29}$$

$$\mathcal{F}_s(V) = u - s[i\hbar\omega_n + \mu]V + s\frac{2i\hbar\omega_n + 2\mu + V}{2i\hbar\omega_n + 2\mu - V}t_\perp^2, \tag{30}$$

where the three variables z^+, z^-, and u are defined by

$$z^+ = \frac{1}{\hbar v_F}\sqrt{(i\hbar\omega_n + \mu)^2 + \frac{V^2}{4} + u}, \tag{31}$$

$$z^- = \frac{1}{\hbar v_F}\sqrt{(i\hbar\omega_n + \mu)^2 + \frac{V^2}{4} - u}, \tag{32}$$

$$u = \sqrt{(i\hbar\omega_n + \mu)^2(V^2 + t_\perp^2) - \frac{V^2t_\perp^2}{4}}. \tag{33}$$

Note that all three square roots are taken so that the imaginary part is positive valued.

TABLE VI. Elements of the finite-temperature Green's function of bilayer graphene in the presence of a layer symmetry-breaking field.

$\alpha_l\alpha'_{l'}$	$\mathcal{M}_{\alpha_l\alpha'_{l'}}(\mathbf{R},E)$
A_1A_1	$2\mathcal{B}(-V)[\mathcal{A}(-V)H_0^1(z^+R)+\mathcal{A}(V)H_0^1(z^-R)]$
A_1B_1	$4i\hbar v_F\Phi_m(\mathbf{R})[\mathcal{A}(-V)z^+H_1^1(z^+R)+\mathcal{A}(V)z^-H_1^1(z^-R)]$
A_1A_2	$t_\perp\mathcal{B}(V)\mathcal{B}(-V)[H_0^1(z^+R)-H_0^1(z^-R)]$
A_1B_2	$2i\hbar v_F\Phi_m^*(\mathbf{R})t_\perp\mathcal{B}(-V)[z^+H_1^1(z^+R)-z^-H_1^1(z^-R)]$
B_1B_1	$2\mathcal{B}(-V)[\mathcal{F}_+(V)H_0^1(z^+R)+\mathcal{F}_-(V)H_0^1(z^-R)]$
B_1A_2	$2i\hbar v_F\Phi_m^*(\mathbf{R})t_\perp\mathcal{B}(V)[z^+H_1^1(z^+R)-z^-H_1^1(z^-R)]$
B_1B_2	$-4\hbar^2v_F^2\Phi_m^{*2}(\mathbf{R})t_\perp[z^{+2}H_2^1(z^+R)-z^{-2}H_2^1(z^-R)]$
A_2A_2	$2\mathcal{B}(V)[\mathcal{A}(V)H_0^1(z^+R)+\mathcal{A}(-V)H_0^1(z^-R)]$
A_2B_2	$4i\hbar v_F\Phi_m^*(\mathbf{R})[\mathcal{A}(V)z^+H_1^1(z^+R)+\mathcal{A}(-V)z^-H_1^1(z^-R)]$
B_2B_2	$2\mathcal{B}(V)[\mathcal{F}_+(-V)H_0^1(z^+R)+\mathcal{F}_-(-V)H_0^1(z^-R)]$

TABLE VII. Intralayer part of the RKKY interaction at finite temperature; the expression for the full RKKY interaction is given in Eq. (34).

$\alpha_l\alpha'_{l'}$	$\mathcal{I}_{\alpha_l\alpha'_{l'}}(R)$	$f_{\alpha\alpha'}(\mathbf{R})$
A_1A_1	$\frac{\pi}{4\hbar^2v_F^2\beta}\sum_n \frac{\mathcal{B}(-V)^2}{u^2}[\mathcal{A}(-V)H_0^1(z^+R)+\mathcal{A}(V)H_0^1(z^-R)]^2$	$f_{A_1A_1}(\mathbf{R})$
A_2A_2	$\frac{\pi}{4\hbar^2v_F^2\beta}\sum_n \frac{\mathcal{B}(V)^2}{u^2}[\mathcal{A}(V)H_0^1(z^+R)+\mathcal{A}(-V)H_0^1(z^-R)]^2$	$f_{A_1A_1}(\mathbf{R})$
B_1B_1	$\frac{\pi}{4\hbar^2v_F^2\beta}\sum_n \frac{\mathcal{B}(-V)^2}{u^2}[\mathcal{F}_+(V)H_0^1(z^+R)+\mathcal{F}_-(V)H_0^1(z^-R)]^2$	$f_{A_1A_1}(\mathbf{R})$
B_2B_2	$\frac{\pi}{4\hbar^2v_F^2\beta}\sum_n \frac{\mathcal{B}(V)^2}{u^2}[\mathcal{F}_+(-V)H_0^1(z^+R)+\mathcal{F}_-(-V)H_0^1(z^-R)]^2$	$f_{A_1A_1}(\mathbf{R})$
B_1A_1	$\frac{\pi}{\beta}\sum_n \frac{1}{u^2}[\mathcal{A}(-V)z^+H_1^1(z^+R)+\mathcal{A}(V)z^-H_1^1(z^-R)]^2$	$f_{B_1A_1}(\mathbf{R})$
A_2B_2	$\frac{\pi}{\beta}\sum_n \frac{1}{u^2}[\mathcal{A}(V)z^+H_1^1(z^+R)+\mathcal{A}(-V)z^-H_1^1(z^-R)]^2$	$f_{B_1A_1}(\mathbf{R})$
B_2A_1	$\frac{\pi t_\perp^2}{4\beta}\sum_n \frac{\mathcal{B}(-V)^2}{u^2}[z^+H_1^1(z^+R)-z^-H_1^1(z^-R)]^2$	$f_{B_1A_1}(-\mathbf{R})$
A_2B_1	$\frac{\pi t_\perp^2}{4\beta}\sum_n \frac{\mathcal{B}(V)^2}{u^2}[z^+H_1^1(z^+R)-z^-H_1^1(z^-R)]^2$	$f_{B_1A_1}(-\mathbf{R})$
A_2A_1	$\frac{\pi t_\perp^2}{16\hbar^2v_F^2\beta}\sum_n \frac{\mathcal{B}(V)^2\mathcal{B}(-V)^2}{u^2}[H_0^1(z^+R)-H_0^1(z^-R)]^2$	$f_{A_1A_1}(\mathbf{R})$
B_2B_1	$\frac{\pi\hbar^2v_F^2t_\perp^2}{\beta}\sum_n \frac{1}{u^2}[z^{+2}H_2^1(z^+R)-z^{-2}H_2^1(z^-R)]^2$	$f_{B_2B_1}(\mathbf{R})$

2. *RKKY interaction*

The RKKY interaction at finite temperature may be obtained from Eq. (4) by direct insertion of the appropriate Green's function, to obtain the ten inequivalent RKKY interactions of the biased bilayer at finite temperature:

$$J_{\alpha_l\alpha'_{l'}}(\mathbf{R}) = C\mathcal{I}_{\alpha_l\alpha'_{l'}}(R)f_{\alpha_l\alpha'_{l'}}(\mathbf{R}). \tag{34}$$

The functions $\mathcal{I}_{\alpha_l\alpha'_{l'}}$ are presented in Table VII.

III. RESULTS

A. Numerical method

Rather than use the $T = 0$ formalism, it turns out to be significantly more numerically efficient to evaluate the finite-temperature formalism RKKY Matsubara sums at a low temperature ($T = 10$ K). This, of course, simply reflects the fact that the Matsubara sums of Table VII are evaluated in the complex plane, while the exchange integrals of Table V are taken on the real axis and, therefore, are highly oscillatory for large impurity separations. For the Matsubara sums we find that 4001 poles are sufficient for convergence of the RKKY interaction for all impurity separations. The RKKY interaction we present, in all results, in terms of the coupling constant C.

B. Coupling scheme

We will consider the RKKY interaction between intercalated impurities, i.e., impurities that occupy one of the open interlayer spaces of the AB-stacked lattice. Our motivation for this choice is that this geometry offers the best chance of significant exchange coupling of the impurity to the electron gas of the bilayer, as evidenced by the fact that intercalation of graphite yields significant such coupling. In this context it is worth noting also that the twist bilayer [32] may present an interesting system for such intercalation [33]. The impurity center is positioned along the vertical vector connecting the center of a honeycomb of one layer and a carbon atom in the second layer and there are, therefore, 10 nearest-neighbor carbon atoms to the impurity (see Fig. 1). The impurity exchange field will be significant only on these nearest-neighbor atoms and if we consider the intercalated impurity RKKY interaction as simply a superposition of all the RKKY interactions between these ten neighboring carbon atoms, the so-called *incoherent coupling scheme*, then there are $10^2 = 100$ substitutional type impurity RKKY interactions that must be summed over.

In contrast to the usual RKKY interaction in which the long-range behavior is determined solely by the Fermi surface, the multivalley nature of the electronic structure in graphene and bilayer-graphene means that the RKKY interaction depends on both the Fermiology and on the local structure of the impurity. The precise nature of the coupling scheme must therefore be considered in any investigation of the RKKY interaction in these materials. For the intercalated impurity there are, in principle, 10 different coupling constants λ_i that must be fixed. These will depend on the detailed electronic structure of the impurity-bilayer interaction, and in particular the orbital structure of the impurity atom, and such information can only be obtained *ab initio* on a case-by-case basis for each impurity type. We will not consider the *ab initio* approach here but rather follow Ref. [25], in which a detailed investigation was performed of how a particular coupling scheme may impact on the long-range RKKY interaction. In that work, in which both the incoherent superposition scheme as well as the so-called *coherent coupling scheme* that involves four-site exchange interactions were considered, it was found that while the form of the RKKY interaction can be qualitatively changed by the coupling scheme, for many cases the simplest incoherent coupling scheme captures the behavior reproduced by a wide range of the more complex coupling schemes. For that reason we will use this scheme here. As in Refs. [25] and [26] we take λ to depend only on the separation of the impurity center and the neighboring carbon atom; in this was we have two parameters, λ_1 and $\lambda_2 = 1.2\lambda_1$. It should also be noted that in Ref. [15] the RKKY interaction of impurities in a

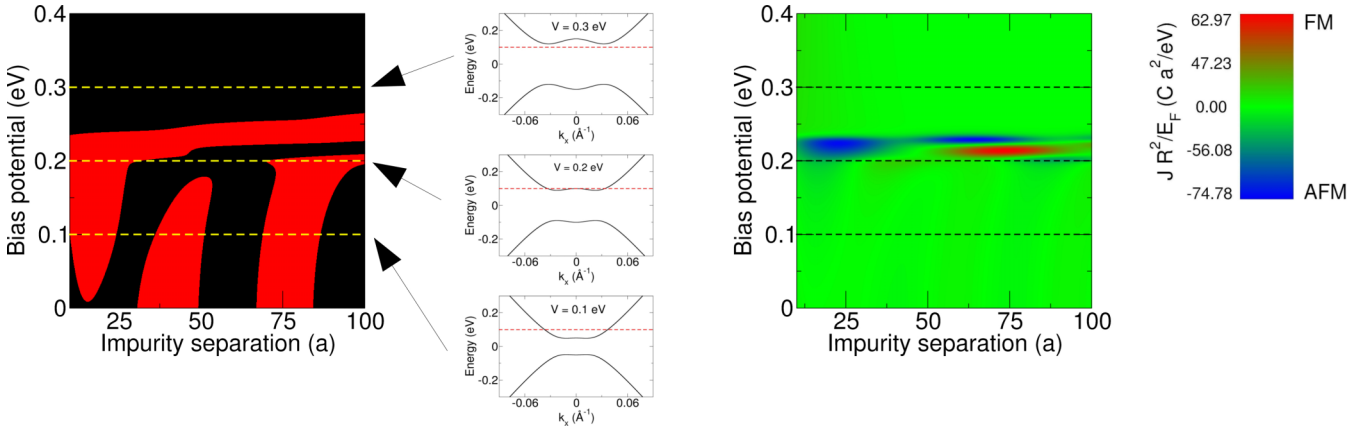

FIG. 4. Overview of the RKKY interaction for a fixed Fermi energy of 100 meV. The left panel presents a density plot of the spin coupling type—ferromagnetic or antiferromagnetic—as a function of impurity separation and interlayer bias. The low-energy band structure for three representative values of this interlayer bias (0.1, 0.2, and 0.3 eV) is displayed in the associated panels indicated by arrows; the dashed lines on the density plots correspond to these bias values. The right panel shows the magnitude of the RKKY interaction plotted over the same variables, with the interaction clearly massively enhanced for values of the interlayer bias that place the Fermi energy in the Mexican hat region. The connection vector between the impurities is assumed to be in the armchair direction, and thus the intervalley scattering factors f [see Eqs. (23)–(25)] are all unity. The temperature is set to 10 K.

plaquette geometry were considered and a ferromagnetic to antiferromagnetic switching shown to be possible by tuning the gate bias; while our work will consider in much more detail both the field and temperature dependence of intercalated impurities, the fact that a sensitive dependence on field is found also for the plaquette geometry supports the view that a diverse range of local coupling schemes are represented by the results presented here.

C. RKKY interaction with a fixed Fermi energy

We will first consider the case in which the Fermi energy is pinned at some fixed level for all values of the interlayer bias, as is the case in graphene epilayers grown by sublimation of Si from the Si face of SiC [34,35]. For that system the dangling bonds of the buffer layer pin the Fermi energy at approximately 0.1 eV, and we will use this value here. Qualitatively similar results, however, are obtained for Fermi energies $0\ \text{eV} < |E_F| < 0.2$ eV, with the only difference that the larger the Fermi energy the greater the interlayer bias required to see the full range of behavior of the RKKY interaction. In Fig. 4 we present an overview of the RKKY interaction for a range of interlayer bias potentials and impurity separations. For a complete picture of the effects of an interlayer bias, we present values up to 0.4 eV, which correspond to a rather high field of 114 mV/Å, although, as may be seen, the interesting effects correspond to much lower physically achievable fields of less than 30 mV/Å.

In the left panel of Fig. 4 the type of coupling—ferromagnetic or antiferromagnetic—is displayed as a density plot for $10a < R < 100a$ and $0\ \text{eV} < V < 0.4$ eV. Three qualitatively different regions as a function of the interlayer bias may be seen: For low bias an oscillatory form of the RKKY is observed, which on increasing the bias becomes an antiferromagnetic interaction for all $R > 10a$, before a ferromagnetic interaction sets in at all impurity separations for $V > 0.26$ eV. These changes are easily correlated with corresponding changes in the band structure of the bilayer that occur due to the applied field, as displayed in the three panels accompanying this figure. For low bias the Fermi energy is in the single-band region, and the Fermi vector k_F of the circular Fermi surface drives an oscillatory RKKY interaction. This behavior is qualitatively similar to that seen for zero bias. Increasing the bias opens the band gap further and the Mexican hat region of the spectrum then crosses the Fermi energy. This band structure is qualitatively different from the low-energy band structure at zero bias, but shares features in common with the band edge of the high-energy antibonding band [25]. In particular, both feature regions in which the band velocity vanishes are associated with zeros of the arguments of the Bessel functions of the integrand of the RKKY forms shown in Table V. These divergences are integrable but lead to a pronounced increase in the RKKY interaction in the Mexican hat region. This may be seen in the right panel of Fig. 4. For interlayer bias greater than $E_F/2 = 50$ meV the Fermi energy is in the band gap and the RKKY is ferromagnetic for all R and assumes an exponential decay.

A closer look at this evolution of RKKY forms as a function of bias is provided in Fig. 5, in which we plot the RKKY interaction as a function of separation for four representative values of bias. Clearly, when the interlayer bias places the Fermi energy in the Mexican hat region, $V = 0.20$ eV and $V = 0.22$ eV, the RKKY interaction is massively enhanced. It is also noteworthy that for the case where the Fermi energy is in the band gap, $V = 0.27$ eV, the RKKY interaction, while possessing an asymptotically exponential decay, is in the region $R < 25a$ comparable or greater in magnitude to the oscillatory RKKY interaction found in the single band ($V = 0.10$ eV).

The rapid change in form of the RKKY interaction observed in the Mexican hat region as a function of energy signals the existence of interesting RKKY physics at finite temperatures. As the temperature is increased the Fermi window k_BT expands to take in energy regions of the propagator having

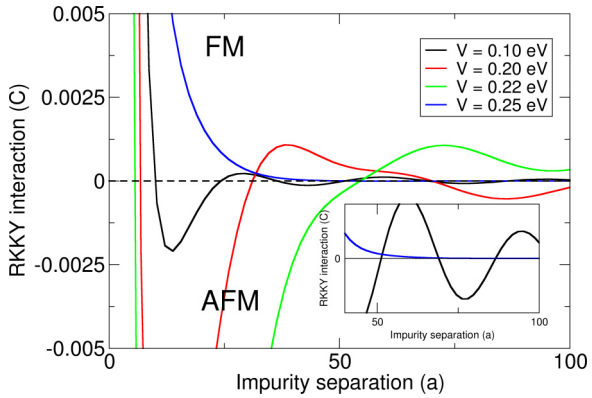

FIG. 5. The RKKY interaction for a fixed Fermi energy of 100 meV and a selection of bias potentials representative of the behavior seen in Fig. 4. The form of the RKKY interaction evolves from oscillatory at low bias, through a massively enhanced antiferromagnetic coupling, to a ferromagnetic form. The RKKY interaction is evaluated at 10 K and the connection vector of the impurities **R** is taken to be in the armchair direction, and thus the intervalley scattering factors [Eqs. (23)–(25)] are all unity.

very different behavior to that found on the $T = 0$ energy shell, and this can lead to dramatic changes in the form of the RKKY interaction as a function of temperature [26]. In Fig. 6 we present the RKKY interaction for a Fermi energy of 100 meV and an interlayer bias of 0.26 eV and calculated as a function of R for temperatures between 10 K and 300 K. The shaded area of the figure signals the region of interest, within which one may observe a change in the form of the RKKY interaction as a function of temperature which evolves from a low-temperature ferromagnetic coupling to a high-temperature antiferromagnetic coupling. This behavior is remarkably at variance with the usual RKKY interaction in which temperature merely suppresses the interaction strength, but does not lead to a change in the form of the interaction [6,9,26,36].

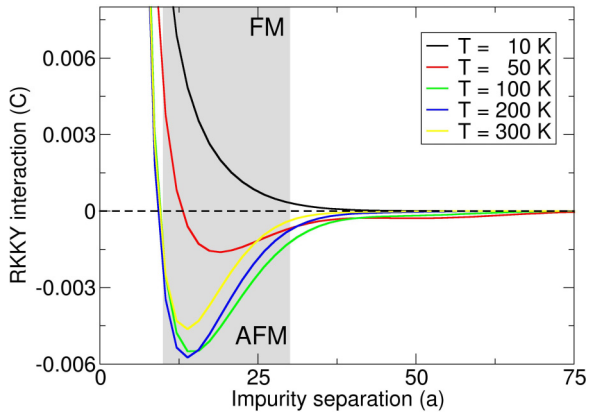

FIG. 6. Effect of finite temperature on the RKKY interaction. The Fermi energy is pinned to a value of 100 meV and the interlayer bias is fixed at 0.26 eV. While the RKKY interaction changes form from antiferromagnetic to ferromagnetic, it does not significantly reduce in magnitude. The connection vector of the impurities **R** is taken to be in the armchair direction and thus the intervalley scattering factors [Eqs. (23)–(25)] are all unity.

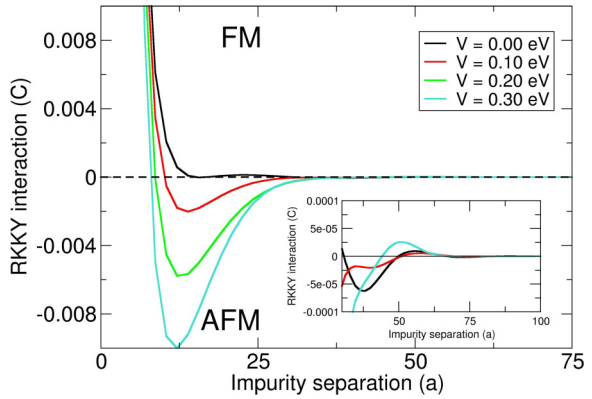

FIG. 7. RKKY interaction at fixed particle density. The particle density at $E_F = 100$ meV and zero bias is maintained for all finite values of the interlayer bias. The inset displays the large R behavior. The connection vector of the impurities **R** is taken to be in the armchair direction and thus the intervalley scattering factors [Eqs. (23)–(25)] are all unity.

D. RKKY interaction at a fixed particle density

How does this physics change if we consider, instead of the Fermi energy, the particle density to be the fixed parameter as the interlayer bias changes? This is the physical scenario which occurs when the bilayer is deposited on a nonpolar insulator. An obvious difference is that increasing the bias can no longer result in a situation in which the Fermi energy is in the band gap; instead the Fermi energy itself changes as the gap opens with increasing bias, such that the particle density is maintained at a fixed value. In Fig. 7 is shown the effect of increasing the interlayer bias from a value of zero. The Fermi energy is set to 100 eV at zero bias, and for all finite bias values the particle density is held fixed at the zero bias density. The most important difference from the previous case we studied (compare with Fig. 5) is that RKKY interaction never evolves to the monotonic ferromagnetic interaction found when the Fermi energy is in the band gap. Instead, once the bias is such that the Fermi energy is in the Mexican hat region it will stay there, and further increases in the bias simply result in a greater strength of the antiferromagnetic coupling for separations $10a < R < 30a$; see Fig. 7.

E. RKKY interaction with the Fermi level pinned at the Dirac point

Finally, we consider the RKKY interaction for the case in which the Fermi energy is pinned at the Dirac point, a situation that arises, for example, in suspended bilayer graphene samples or bilayer graphene deposited on SiO_2. In the absence of an applied bias the RKKY interaction at the Dirac point for intercalated impurities is antiferromagnetic for $R > 14a$ and with a monotonic R^{-2} asymptotic decay envelope [25]. When the interlayer bias is switched on the Fermi energy immediately enters the gap. The RKKY interaction, however, smoothly evolves in the near-field region and evolves from an antiferromagnetic to a ferromagnetic interaction, as may be seen in Fig. 8.

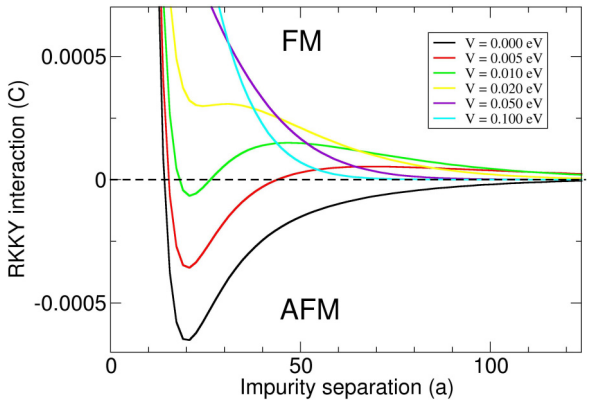

FIG. 8. The RKKY interaction at the Dirac point for a range of bias potentials, $T = 10$ K. The connection vector of the impurities **R** is taken to be in the armchair direction, and thus the intervalley scattering factors [Eqs. (23)–(25)] are all unity.

IV. SUMMARY AND CONCLUSIONS

We find that the RKKY interaction of the Bernal stacked bilayer may be tuned between a variety of qualitatively different forms by application of a layer symmetry-breaking field. We consider three scenarios within which this can be realized: (i) a Fermi energy pinned at a value similar to that found in graphene on the (0001) face of SiC, (ii) a fixed particle density, and (iii) a Fermi energy pinned at the Dirac point. For the SiC scenario we find the RKKY interaction in zero bias assumes an oscillatory form, but that this can be tuned to be antiferromagnetic by increasing the bias, with the magnitude of the interaction enhanced by almost an order of magnitude. Higher values of the bias result in the Fermi energy entering the band gap and a ferromagnetic RKKY interaction with an asymptotic exponential decay. Thus, simply by tuning an applied field we can access the full range of interaction types: oscillatory, antiferromagnetic, and ferromagnetic. For the case in which the particle density is fixed a similar behavior is seen, with the key difference that the gap region ferromagnetic coupling is never reached; instead increasing the interlayer bias simply increases in strength the antiferromagnetic interaction for impurity separations $10a < R < 40a$.

In the case in which the Fermi energy is pinned at the Dirac point we find that the RKKY interaction evolves from antiferromagnetic to ferromagnetic with applied bias. As soon as the bias is switched on the Fermi enters resides within the band gap, and the asymptotic decay of the RKKY interaction is exponential. This exponential decay might be thought to indicate a much reduced strength of the RKKY interaction. However, for impurity separations $R < 60a$ the magnitude of the ferromagnetic RKKY interaction at an interlayer bias of 50 meV is comparable to that of the antiferromagnetic interaction found at zero bias.

In conclusion, we find that the RKKY interaction in bilayer graphene exhibits a number of ways in which it may be manipulated with an external field, both in the case of a pinned Fermi energy as well as the case of a fixed electron density. Bilayer graphene heterostructures formed from a dilute intercalation of magnetic impurities may therefore represent a system in which, by tuning an applied field, a considerable degree of control may be exercised over the magnetic structure.

ACKNOWLEDGMENTS

This work was supported by the Collaborative Research Center SFB 953 of the Deutsche Forschungsgemeinschaft (DFG).

[1] M. A. Ruderman and C. Kittel, Indirect exchange coupling of nuclear magnetic moments by conduction electrons, Phys. Rev. **96**, 99 (1954).
[2] Tadao Kasuya, A theory of metallic ferro- and antiferromagnetism on zener's model, Prog. Theor. Phys. **16**, 45 (1956).
[3] Kei Yosida, Magnetic properties of cu-mn alloys, Phys. Rev. **106**, 893 (1957).
[4] Saeed Saremi, Rkky in half-filled bipartite lattices: Graphene as an example, Phys. Rev. B **76**, 184430 (2007).
[5] E. H. Hwang and S. Das Sarma, Screening, Kohn Anomaly, Friedel Oscillation, and Rkky Interaction in Bilayer Graphene, Phys. Rev. Lett. **101**, 156802 (2008).
[6] J. E. Bunder and Hsiu-Hau Lin, Ruderman-kittel-kasuya-yosida interactions on a bipartite lattice, Phys. Rev. B **80**, 153414 (2009).
[7] A. M. Black-Schaffer, Importance of electron-electron interactions in the RKKY coupling in graphene, Phys. Rev. B **82**, 073409 (2010).
[8] A. M. Black-Schaffer, RKKY coupling in graphene, Phys. Rev. B **81**, 205416 (2010).
[9] Thomas Fabritius, Nicolas Laflorencie, and Stefan Wessel, Finite-temperature ordering of dilute graphene antiferromagnets, Phys. Rev. B **82**, 035402 (2010).
[10] M. Sherafati and S. Satpathy, Analytical expression for the RKKY interaction in doped graphene, Phys. Rev. B **84**, 125416 (2011).
[11] Bruno Uchoa, T. G. Rappoport, and A. H. Castro Neto, Kondo Quantum Criticality of Magnetic Adatoms in Graphene, Phys. Rev. Lett. **106**, 016801 (2011).
[12] Karol Szalkowski, RKKY coupling between impurity spins in graphene nanoflakes, Phys. Rev. B **84**, 205409 (2011).
[13] E. Kogan, RKKY interaction in graphene, Phys. Rev. B **84**, 115119 (2011).
[14] M. Sherafati and S. Satpathy, RKKY interaction in graphene from the lattice Green's function, Phys. Rev. B **83**, 165425 (2011).
[15] Matthew Killi, Dariush Heidarian, and Arun Paramekanti, Controlling local moment formation and local moment interactions in bilayer graphene, New J. Phys. **13**, 053043 (2011).
[16] Liwei Jiang, Xiaoling Lü, Wenzhu Gao, Guodong Yu, Zhe Liu, and Yisong Zheng, Rkky interaction in ab-stacked multilayer graphene, J. Phys.: Condens. Matter **24**, 206003 (2012).
[17] S. R. Power, F. S. M. Guimarães, A. T. Costa, R. B. Muniz, and M. S. Ferreira, Dynamic RKKY interaction in graphene, Phys. Rev. B **85**, 195411 (2012).

[18] Hyunyong Lee, Junghoon Kim, E. R. Mucciolo, Georges Bouzerar, and S. Kettemann, RKKY interaction in disordered graphene, Phys. Rev. B **85**, 075420 (2012).

[19] Hyunyong Lee, E. R. Mucciolo, Georges Bouzerar, and S. Kettemann, RKKY interaction in disordered graphene, Phys. Rev. B **86**, 205427 (2012).

[20] Alireza Habibi and S. A. Jafari, RKKY interaction in heavily vacant graphene, J. Phys.: Condens. Matter, **25**, 375501 (2013).

[21] F. Parhizgar, M. Sherafati, R. Asgari, and S. Satpathy, Ruderman-kittel-kasuya-yosida interaction in biased bilayer graphene, Phys. Rev. B **87**, 165429 (2013).

[22] F. Parhizgar, Reza Asgari, Saeed H. Abedinpour, and M. Zareyan, Anisotropic RKKY interaction in spin-polarized graphene, Phys. Rev. B **87**, 125402 (2013).

[23] J. H. Sun, F. M. Hu, H. K. Tang, W. Guo, and H. Q. Lin, Indirect exchange of magnetic impurities in zigzag graphene ribbon, J. Appl. Phys. **113**, 17B515 (2013).

[24] P. D. Gorman, J. M. Duffy, M. S. Ferreira, and S. R. Power, RKKY interaction between adsorbed magnetic impurities in graphene: Symmetry and strain effects, Phys. Rev. B **88**, 085405 (2013).

[25] N. Klier, S. Shallcross, and O. Pankratov, Asymptotic discontinuities in the RKKY interaction in the graphene bernal bilayer, Phys. Rev. B **90**, 245118 (2014).

[26] N. Klier, S. Shallcross, S. Sharma, and O. Pankratov, Ruderman-kittel-kasuya-yosida interaction at finite temperature: Graphene and bilayer graphene, Phys. Rev. B **92**, 205414 (2015).

[27] Alexander Ako Khajetoorians, Jens Wiebe, Bruno Chilian, Samir Lounis, Stefan Blügel, and Roland Wiesendanger, Atom-by-atom engineering and magnetometry of tailored nanomagnets, Nat. Phys. **8**, 497 (2012).

[28] Edward McCann, Asymmetry gap in the electronic band structure of bilayer graphene, Phys. Rev. B **74**, 161403 (2006).

[29] E. V. Castro, K. S. Novoselov, S. V. Morozov, N. M. R. Peres, J. M. B. dos Santos Lopes, J. Nilsson, F. Guinea, A. K. Geim, and A. H. Castro Neto, Biased Bilayer Graphene: Semiconductor with a Gap Tunable by the Electric Field Effect, Phys. Rev. Lett. **99**, 216802 (2007).

[30] Johan Nilsson, A. H. Castro Neto, F. Guinea, and N. M. R. Peres, Electronic properties of bilayer and multilayer graphene, Phys. Rev. B **78**, 045405 (2008).

[31] Eduardo V. Castro, K. S. Novoselov, S. V. Morozov, N. M. R. Peres, J. M. B. Lopes dos Santos, Johan Nilsson, F. Guinea, A. K. Geim, and A. H. Castro Neto, Electronic properties of a biased graphene bilayer, J. Phys.: Condens. Matter **22**, 175503 (2010).

[32] S. Shallcross, S. Sharma, and O. Pankratov, Emergent momentum scale, localization, and van hove singularities in the graphene twist bilayer, Phys. Rev. B **87**, 245403 (2013).

[33] Franz Symalla, Sam Shallcross, Igor Beljakov, Karin Fink, Wolfgang Wenzel, and Velimir Meded, Band-gap engineering with a twist: Formation of intercalant superlattices in twisted graphene bilayers, Phys. Rev. B **91**, 205412 (2015).

[34] Shinichi Tanabe, Yoshiaki Sekine, Hiroyuki Kageshima, Masao Nagase, and Hiroki Hibino, Carrier transport mechanism in graphene on SiC(0001), Phys. Rev. B **84**, 115458 (2011).

[35] N. Ray, S. Shallcross, S. Hensel, and O. Pankratov, Buffer layer limited conductivity in epitaxial graphene on the Si face of SiC, Phys. Rev. B **86**, 125426 (2012).

[36] V. I. Litvinov and V. K. Dugaev, RKKY interaction in one- and two-dimensional electron gases, Phys. Rev. B **58**, 3584 (1998).